Journal of Solid Mechanics Vol. 1, No. 3 (2009) pp. 245-259

hp-Spectral Finite Element Analysis of Shear Deformable Beams and Plates

Rakesh Ranjan, J.N. Reddy*

Advanced Computational Mechanics Laboratory, Department of Mechanical Engineering, Texas A&M University, College Station, TX 77843-3123, USA

Received 25 November 2009; accepted 30 November 2009

ABSTRACT

There are different finite element models in place for predicting the bending behavior of shear deformable beams and plates. Mostly, the literature abounds with traditional equi-spaced Langrange based low order finite element approximations using displacement formulations. However, the finite element models of Timoshenko beams and Mindlin plates with linear interpolation of all generalized displacements have suffered from shear locking, which has been alleviated with the help of primarily reduced/selective integration techniques to obtain acceptable solutions [1-4]. These kinds of 'fixes' have come into existence because the element stiffness matrix becomes excessively stiff with low-order interpolation functions. In this study we propose an alternative spectrally accurate *hp*/spectral method to model the Timoshenko beam theory and first order shear deformation theory of plates (FSDT) to eliminate shear and membrane locking. Beams and isotropic and orthotropic plates with clamped and simply supported boundary conditions are analyzed to illustrate the accuracy and robustness of the developed elements. Full integration scheme is employed for all cases. The results are found to be in excellent agreement with those published in literature.

Keywords: *hp*-Spectral; Finite element analysis; Beams; Plates

1 INTRODUCTION

STUDYING the stress and deformation of beams and plates is of interest in many applications of engineering. Examples of applications are in geotechnical engineering, structural design of foundations, design of spread footings, soil-structure interaction studies, aerospace vehicles, automobiles, etc. Among theories used to analyze plates, classical, first-order, and third-order theories dominate the literature [1, 2]. While the displacement based models for the first-order shear deformation theory (FSDT) admit the use of C^0 expansions, the use of classical and the Reddy third-order theories require the use of C^1-continuous expansions [1,3-6]. The classical plate theory does not account for the transverse shear strains, and therefore the results are inadequate for the prediction of the global response of thick plates. When using the first-order shear deformation theory (FSDT) to model plates, shear correction factors are introduced to correct for the discrepancy between the actual parabolic transverse shear stress distribution and those predicted by the kinematic assumptions of the FSDT. Higher-order plate theories provide a slight increase in the accuracy relative to the FSDT solution, but at the expense of a significant increase in the computational effort. Based on the above arguments the FSDT provides the best compromise between economy, simplicity, and accuracy in prediction of the global response of thin to moderately thick plates [7].

The displacement finite element models of the first-order shear deformation theory have met with locking problems when low- and equal-order interpolations of the generalized displacements are used. This is primarily due to the inconsistent and low order interpolation of different displacement variables. While studies have been carried out with equi-spaced, higher-order Langrange expansions for studying the bending response of plates using FSDT

* Corresponding author.
E-mail address: jnreddy@tamu.edu (J.N. Reddy).

[8], the elements suffer from ill-conditioning and for high polynomial orders the equi-spaced Lagrange based expansion is not recommended [9]. It has been mentioned in literature that polynomial order (p) higher than 4 is not recommended. At high p-levels the discrete problem suffers from a very high conditioning of the stiffness matrix, and strong pre-conditioners recommended to parse the discrete problem at such high p-levels but the convergence is problem dependent and also dependent on the regularity of the mesh. It was discovered in the 1980s that the choice of higher-order shape functions has a dramatic effect on the conditioning of the discrete problem. Since then, significant amount of work has been devoted to the improvement of higher-order shape functions on various types of finite elements. The search for optimality continues till today [10]. Thus, when higher-order shape functions are used in the finite element method, it is common to examine the condition numbers of the coefficient matrix generated. Condition numbers close to one represent a well-conditioned system where as a large condition number indicates a poorly conditioned system of equations which is likely to lead to numerical errors in the solution process. The usual definition of the condition number is being used in the present context, that is.

The *hp*-spectral based nodal expansions which is based on Legendre polynomials provide discrete orthogonality and it has been mentioned that the condition number for the mass matrix of the Langrange based expansions grows as 10^p for higher values of p where as the condition number for the Legendre based expansions grows as O(p). The superior conditioning of both the mass and stiffness matrices produced with the Gauss-Lobatto-Legendre based shape functions has been demonstrated in the following references [10, 11]. The paper by Maitre et al. [11] provides the condition number of the Legendre based expansions to a polynomial order of 30 in 2-dimensions and 9 in three dimensions. The above arguments exhibit the fact that Langrage based higher-order elements suffer from strong linear dependence of the solution and special solution techniques have to be used to address the problem unless one contends with spurious results from the discrete model, reasonable solutions to certain problems only under very special circumstances, or ad-hoc approaches that ameliorate solver breakdowns. In the case of shear deformable beams, so-called consistent interpolation has been used to recover the correct constraints (i.e., vanishing of transverse shear strain) in the thick beam limit [12]. Although such elements do not experience locking, they did not lead to the two-node super-convergent element developed by Reddy et al. [13], who used the Hermite cubic interpolation of the transverse deflection w and *interdependent* quadratic interpolation of the rotation φ in developing the element. The conventional reduced integration Timoshenko elements as well as consistent interpolated quadratic elements fail to capture the true behavior of such members unless two or more elements per a structural member are used. Shear locking is more pre-dominant when the side-to-thickness ratio of the plate is large. Higher-order elements have been explored in literature to alleviate shear locking but they have employed equi-spaced Langrange functions so far. The use of *hp*-spectral nodal expansion was explored by Pontaza and Reddy [6] while analyzing plates with both the classical plate theory and the FSDT with the least squares finite element formulation; however, only a linear analysis was performed. The aforementioned reasons compel the use of *hp*-element refinements as a viable alternative in studying the bending behavior of plates that provides spectrally accurate results while alleviating locking associated with lower order finite elements. This study proposes to advance the use of appropriate *hp*-refinements for studying the plate bending behavior and cures the problem of locking for all cases that are studied.

The motivation for this study comes from the many advantages that are associated with *hp*-higher order elements; spectral convergence (accuracy) of the solutions, the removal of shear as well as membrane locking, and the orthogonality property of nodal expansions, which provide excellent results with standard solvers like the preconditioned bi-orthogonal conjugate gradient (BPCG) methods. The convergence history of the bi-orthogonal conjugate gradient solver with preconditioning is also reported to give further insight into the problem formulation and convergence behavior with *hp*-spectral methods. Different a/h ratios are explored and with appropriate *hp*-refinements, and full integration is found to provide consistently good agreement with published results. Both straight and skewed *hp*-spectral meshes are explored in this study of plates and it is found that there is no drastic deterioration in the results when using skewed meshes.

2 FINITE ELEMENT MODELS BEAMS

2.1 Governing equations

The equations governing the bending of beams according to the Timoshenko beam theory (TBT) are can be expressed in terms of the axial displacement u_0, transverse displacement w_0, rotation φ_x, and stress resultants (N_{xx}, M_{xx}, Q_x) as [3]

$$\frac{\mathrm{d}N_{xx}}{\mathrm{d}x}+f_x=0 \tag{1}$$

$$\frac{\mathrm{d}M_{xx}}{\mathrm{d}x}-Q_x=0 \tag{2}$$

$$\frac{\mathrm{d}Q_x}{\mathrm{d}x}+\frac{\mathrm{d}}{\mathrm{d}x}\left(N_{xx}\frac{\mathrm{d}w_0}{\mathrm{d}x}\right)+q=0 \tag{3}$$

where the stress resultants (N_{xx}, M_{xx}, Q_x) can be expressed in terms of the displacement gradients as

$$N_{xx}=EA\left[\frac{\mathrm{d}u_0}{\mathrm{d}x}+\frac{1}{2}\left(\frac{\mathrm{d}w_0}{\mathrm{d}x}\right)^2\right] \tag{4}$$

$$M_{xx}=EI\frac{\mathrm{d}\varphi_x}{\mathrm{d}x} \tag{5}$$

$$Q_x=S_{xx}\left(\frac{\mathrm{d}w_0}{\mathrm{d}x}+\varphi_x\right) \tag{6}$$

Here (A_{xx}, D_{xx}, S_{xx}) denote the axial, bending, and shear stiffnesses, respectively,

$$(A_{xx}, D_{xx})=\int_A E(1, z^2)\,\mathrm{d}A=(EA, EI),\quad S_{xx}=K_s\int_A G\,\mathrm{d}A=K_sGA=\frac{K_sEA}{2(1+\nu)} \tag{7}$$

E being the modulus of elasticity, A the area of cross section, and I the second moment of area of the beam; (f_x, q) denote the axial and transverse distributed loads. The boundary conditions involve specification of one element of the following pairs of displacements and forces [3, 14]:

$$(u_0, N_{xx}),\quad (w_0, V_x),\quad (\varphi_x, M_{xx})\qquad \text{where}\quad V_x=Q_x+N_{xx}\frac{dw_0}{dx} \tag{8}$$

The non-linearity in the TBT comes from the von Karman non-linear strains as a form of geometric non-linearity.

2.2 Finite element model

The displacement finite element model of the TBT has been outlined in [3] and therefore omitted here in the interest of brevity. A mixed finite element model of the TBT is presented here. The mixed finite element model of TBT is based on Eqs. (1) through (6). The weak form statements of Eqs. (1)-(6) are [14]

$$0=\int_{x_a}^{x_b}\left(\frac{\mathrm{d}\delta u_0}{\mathrm{d}x}N_{xx}-\delta u_0 f_x\right)\mathrm{d}x-\delta u_0(x_a)N_1-\delta u_0(x_b)N_n \tag{9}$$

$$0=\int_{x_a}^{x_b}\left(\frac{\mathrm{d}\delta w_0}{\mathrm{d}x}Q_x+\frac{\mathrm{d}\delta w_0}{\mathrm{d}x}N_{xx}\frac{\mathrm{d}w_0}{\mathrm{d}x}\right)\mathrm{d}x-\delta w_0(x_a)Q_1-\delta w_0(x_b)Q_n \tag{10}$$

$$0=\int_{x_a}^{x_b}\left(\frac{\mathrm{d}\delta\varphi_x}{\mathrm{d}x}M_{xx}+\delta\varphi_x Q_x\right)\mathrm{d}x-\delta\varphi_x(x_a)M_1-\delta\varphi_x(x_b)M_n \tag{11}$$

$$0=\int_{x_a}^{x_b}\delta N_{xx}\left\{N_{xx}-EA\left[\frac{\mathrm{d}u_0}{\mathrm{d}x}+\frac{1}{2}\left(\frac{\mathrm{d}w_0}{\mathrm{d}x}\right)^2\right]\right\}\mathrm{d}x \tag{12}$$

$$0=\int_{x_a}^{x_b}\delta Q_x\left[Q_x-S_{xx}\left(\frac{\mathrm{d}w_0}{\mathrm{d}x}+\varphi_x\right)\right]\mathrm{d}x \tag{13}$$

$$0=\int_{x_a}^{x_b}\delta M_{xx}\left(M_{xx}-EI\,\frac{\mathrm{d}\varphi_x}{\mathrm{d}x}\right)\mathrm{d}x \tag{14}$$

where

$$\begin{aligned}&N_1=-N_{xx}(x_a),\ N_n=N_{xx}(x_b),\ M_1=-M_{xx}(x_a),\ M_n=M_{xx}(x_b)\\&Q_1=-Q_x(x_a),\ Q_n=Q_x(x_b)\end{aligned} \tag{15}$$

To obtain the finite element model, equal interpolation of all six variables $(u_0, w_0, \varphi_x, N_{xx}, Q_x, M_{xx})$ is used:

$$\begin{aligned}&u_0(x)=\sum_{j=1}^{n}u_j\psi_j(x),\ w_0(x)=\sum_{j=1}^{n}w_j\psi_j(x),\ \varphi_x(x)=\sum_{j=1}^{n}S_j\psi_j(x)\\&N_{xx}(x)=\sum_{j=1}^{n}N_j\psi_j(x), Q_x(x)=\sum_{j=1}^{n}V_j\psi_j(x), M_{xx}(x)=\sum_{j=1}^{n}M_j\psi_j(x)\end{aligned} \tag{16}$$

The finite element equations are of the form

$$\begin{bmatrix}\mathbf{K}^{11}&\mathbf{K}^{12}&\mathbf{K}^{13}&\mathbf{K}^{14}&\mathbf{K}^{15}&\mathbf{K}^{16}\\\mathbf{K}^{21}&\mathbf{K}^{22}&\mathbf{K}^{23}&\mathbf{K}^{24}&\mathbf{K}^{25}&\mathbf{K}^{26}\\.&.&.&.&.&.\\.&.&.&.&.&.\\\mathbf{K}^{51}&\mathbf{K}^{52}&.&.&\mathbf{K}^{55}&\mathbf{K}^{56}\\\mathbf{K}^{61}&\mathbf{K}^{62}&\mathbf{K}^{63}&\mathbf{K}^{64}&\mathbf{K}^{65}&\mathbf{K}^{66}\end{bmatrix}\begin{Bmatrix}\mathbf{u}\\\mathbf{w}\\\mathbf{s}\\\mathbf{N}\\\mathbf{V}\\\mathbf{M}\end{Bmatrix}=\begin{Bmatrix}\mathbf{F}^1\\\mathbf{F}^2\\\mathbf{F}^3\\\mathbf{F}^4\\\mathbf{F}^5\\\mathbf{F}^6\end{Bmatrix}\qquad\text{or}\qquad\mathbf{K}\,\boldsymbol{\Delta}=\mathbf{F} \tag{17}$$

where the nonzero stiffness coefficients $\left(K_{ij}^{\alpha\beta}, F_i^{\alpha}\right)$ are given by

$$\begin{aligned}&K_{ij}^{14}=\int_{x_a}^{x_b}\frac{d\psi_i}{dx}\psi_j\,\mathbf{d}x\ , F_i^1=\int_{x_a}^{x_b}\psi_i f_x\mathbf{d}x+\psi_i(x_a)N_1+\psi_i(x_b)N_n,\\&K_{ij}^{24}=\int_{x_a}^{x_b}\frac{dw_0}{dx}\frac{d\psi_i}{dx}\psi_j\,\mathbf{d}x\ , K_{ij}^{25}=\int_{x_a}^{x_b}\frac{d\psi_i}{dx}\psi_j\,\mathbf{d}x\ , F_i^2=\int_{x_a}^{x_b}\psi_i q\,\mathbf{d}x+\psi_i(x_a)Q_1+\psi_i(x_b)Q_n\\&K_{ij}^{35}=\int_{x_a}^{x_b}\psi_i\psi_j\,\mathbf{d}x,\ K_{ij}^{36}=\int_{x_a}^{x_b}\frac{d\psi_i}{dx}\psi_j\,\mathbf{d}x,\ F_i^3=\psi_i(x_a)M_1+\psi_i(x_b)M_n\\&K_{ij}^{41}=-\int_{x_a}^{x_b}EA\,\psi_i\frac{\mathbf{d}\psi_j}{\mathbf{d}x}\mathbf{d}x,\ K_{ij}^{42}=-\frac{1}{2}\int_{x_a}^{x_b}EA\,\frac{\mathbf{d}w_0}{\mathbf{d}x}\psi_i\frac{\mathbf{d}\psi_j}{\mathbf{d}x}\mathbf{d}x,\ K_{ij}^{44}=\int_{x_a}^{x_b}\psi_i\psi_j\,\mathbf{d}x\\&K_{ij}^{52}=-\int_{x_a}^{x_b}K_sGA\,\psi_i\frac{\mathbf{d}\psi_j}{\mathbf{d}x}\mathbf{d}x,\ K_{ij}^{53}=-\int_{x_a}^{x_b}K_sGA\,\psi_i\psi_j\,\mathbf{d}x,\ K_{ij}^{55}=\int_{x_a}^{x_b}\psi_i\psi_j\,\mathbf{d}x\\&K_{ij}^{63}=-\int_{x_a}^{x_b}EI\,\psi_i\frac{\mathbf{d}\psi_j}{\mathbf{d}x}\mathbf{d}x,\ K_{ij}^{66}=\int_{x_a}^{x_b}\psi_i\psi_j\,\mathbf{d}x\end{aligned} \tag{18}$$

Note that the coefficient matrix $\mathbf{K}$ is nonlinear on account of the geometric nonlinearity.

2.3 Spectral/hp Element Formulation

The mixed finite element model of the TBT involves the solution of six degrees of freedom per node $(u_0, w_0, \varphi_x, N_{xx}, Q_x, M_{xx})$. In the spectral approximation, the approximation functions ψ_i are given by [9]

$$\psi_j = \frac{(\varsigma-1)(\varsigma+1)L_p^{'}(\varsigma)}{p(p+1)L_p(\varsigma_i)(\varsigma-\varsigma_p)} \tag{19}$$

where $L_p=P_p^{(0,0)}$ is the Legendre polynomial of order p, and ζ_i denotes the roots of the equation $(\zeta\text{-}1)(\zeta\text{+}1)L_p'(\zeta)= 0$ in the interval [-1, +1]. All Legendre polynomials, $P_n^{\alpha,\beta}$, satisfy a three-term recurrence relation of the form:

$$xP_n^{\alpha,\beta} = a_{n,-1,n}^{\alpha,\beta}P_{n-1}^{\alpha,\beta}(x) + a_{n,n}^{\alpha,\beta}P_n^{\alpha,\beta}(x) + a_{n+1,n}^{\alpha,\beta}P_{n+1}^{\alpha,\beta}(x) \tag{20}$$

where, $a^{\alpha,\beta}$ only depends on α, β, and n. The derivatives of the Legendre polynomials satisfy a three-term recurrence relation of the form [15, 16]

$$xP_n^{\alpha,\beta} = a_{n,-1,n}^{\alpha,\beta}P_{n-1}^{\alpha,\beta}(x) + a_{n+1,n}^{\alpha,\beta}P_{n+1}^{\alpha,\beta}(x) \tag{21}$$

For the special case of α, β=1, we drop the superscript and the above equation can be written as

$$xP_n = a_1(n)P_{n-1}(x) + a_2(n)P_{n+1}(x) \tag{22}$$

where

$$a_1(n) = \frac{n+1}{2n+3}, \quad a_2(n) = \frac{(n+1)(n+3)}{(2n+1)(2n+3)} \tag{23}$$

All Legendre polynomials satisfy the three terms recurrence relationship of the form

$$(1-x^2)\frac{dP_n^{\alpha,\beta}}{dx} = c_{n-1,n}^{\alpha,\beta}(n)P_{n-1}^{\alpha,\beta}(x) + c_{n+1,n}^{\alpha,\beta}(n)P_{n-1}^{\alpha,\beta}(x) \tag{24}$$

Seeking the recurrance relation for the derivative, we rewrite the above equation by dropping α, and β, for the special case of α, β=1;

$$(1-x^2)\frac{dP_n}{dx} = c_1(n)P_{n-1}(x) + c_2(n)P_{n+!}(x) \tag{25}$$

where

$$c_1(n) = \frac{(n+1)(n+3)}{2n+3}, \qquad c_2(n) = \frac{2n(n+1)(n+3)}{(2n+3)(2n+4)} \tag{26}$$

For an illustration of the proofs of these equalities see Osilenker [16].

3 FINITE ELEMENT MODELS OF PLATES

3.1 Governing equations

The first order shear deformation theory extends the kinematics of the classical plate theory by relaxing the normality restriction on the plate and allows for arbitrary but constant rotations on the transverse normal. The displacement field of the first order shear deformation theory is given by [1-3, 14]

$$\begin{aligned} u(x,y,z) &= u_0(x,y) + z\,\varphi_x(x,y) \\ v(x,y,z) &= v_0(x,y) + z\,\varphi_y(x,y) \\ w(x,y,z) &= w_0(x,y,z) \end{aligned} \tag{27}$$

where u_0, v_0, and w_0 denote the mid-plate displacements and φ_x and, φ_y are the rotations of the transverse normals about the y and x-axes, respectively. The displacement field in Eq. (27) results in the following strain field:

$$\begin{Bmatrix} \varepsilon_{xx} \\ \varepsilon_{yy} \\ \gamma_{yz} \\ \gamma_{xz} \\ \gamma_{xy} \end{Bmatrix} = \begin{Bmatrix} \varepsilon^0_{xx} \\ \varepsilon^0_{yy} \\ \gamma^0_{yz} \\ \gamma^0_{xz} \\ \gamma^0_{xy} \end{Bmatrix} + z \begin{Bmatrix} \varepsilon^1_{xx} \\ \varepsilon^1_{yy} \\ 0 \\ 0 \\ \gamma^1_{xy} \end{Bmatrix} = \begin{Bmatrix} \dfrac{\partial u_0}{\partial x} + \dfrac{1}{2}\left(\dfrac{\partial w_0}{\partial x}\right)^2 \\ \dfrac{\partial v_0}{\partial y} + \dfrac{1}{2}\left(\dfrac{\partial w_0}{\partial y}\right)^2 \\ \dfrac{\partial w_0}{\partial y} + \varphi_y \\ \dfrac{\partial w_0}{\partial x} + \varphi_x \\ \dfrac{\partial u_0}{\partial y} + \dfrac{\partial v_0}{\partial x} + \dfrac{\partial w_0}{\partial x}\dfrac{\partial w_0}{\partial y} \end{Bmatrix} + z \begin{Bmatrix} \dfrac{\partial \varphi_x}{\partial x} \\ \dfrac{\partial \varphi_y}{\partial y} \\ 0 \\ 0 \\ \dfrac{\partial \varphi_x}{\partial y} + \dfrac{\partial \varphi_y}{\partial x} \end{Bmatrix} \tag{28}$$

The virtual work statement for the FSDT is equivalent to the weak form of the governing differential equations. For details on the virtual work principle, the reader is referred to [1-3, 17]. The principle of virtual displacements leads to the following equilibrium (Euler-Lagrange) equations for the FSDT:

$$\frac{\partial N_{xx}}{\partial x} + \frac{\partial N_{xy}}{\partial y} = 0 \tag{29}$$

$$\frac{\partial N_{xy}}{\partial x} + \frac{\partial N_{yy}}{\partial y} = 0 \tag{30}$$

$$\frac{\partial Q_x}{\partial x} + \frac{\partial Q_y}{\partial y} + \frac{\partial}{\partial x}\left(N_{xx}\frac{\partial w_0}{\partial x} + N_{xy}\frac{\partial w_0}{\partial y}\right) + \frac{\partial}{\partial y}\left(N_{xy}\frac{\partial w_0}{\partial x} + N_{yy}\frac{\partial w_0}{\partial y}\right) + q = 0 \tag{31}$$

$$\frac{\partial M_{xx}}{\partial x} + \frac{\partial M_{xy}}{\partial y} - Q_x = 0 \tag{32}$$

$$\frac{\partial M_{xy}}{\partial x} + \frac{\partial M_{yy}}{\partial y} - Q_y = 0 \tag{33}$$

where (N, M, Q) denote the stress resultants

$$\begin{aligned} (N_{xx}, N_{yy}, N_{xy}) &= \int_{-h/2}^{h/2} (\sigma_{xx}, \sigma_{yy}, \sigma_{xy})\,\mathbf{d}z \\ (M_{xx}, M_{yy}, M_{xy}) &= \int_{-h/2}^{h/2} z\,(\sigma_{xx}, \sigma_{yy}, \sigma_{xy})\,\mathbf{d}z \\ (Q_x, Q_y) &= K_s \int_{-h/2}^{h/2} (\sigma_{xz}, \sigma_{yz})\,\mathbf{d}z \end{aligned} \tag{34}$$

The boundary conditions for the FSDT involve specification of one element of the following pairs [1-3]:

$$(u_n, N_{nn}),\ (u_s, N_{ns}),\ (w_0, Q_n),\ (\varphi_n, M_n),\ (\varphi_s, M_{ns}) \tag{35}$$

where quantities with subscript `n' denote those acting along the normal on an edge whose normal is $\hat{\mathbf{n}}$, and quantities with subscripts `ns' are those tangential to the edge. Again, the non-linearity in the FSDT comes from the von Karman non-linear strains given in Eq. (28). The plate constitutive equations relate the stress resultants to the strains in Eq. (28). For orthotropic plates with material axes coinciding with the (x, y, z) coordinates, we have [1-3]

$$\begin{Bmatrix} N_{xx} \\ N_{yy} \\ N_{xy} \end{Bmatrix} = \begin{bmatrix} A_{11} & A_{12} & 0 \\ A_{12} & A_{22} & 0 \\ 0 & 0 & A_{66} \end{bmatrix} \begin{Bmatrix} \varepsilon^0_{xx} \\ \varepsilon^0_{yy} \\ \gamma^0_{xy} \end{Bmatrix}, \quad \begin{Bmatrix} M_{xx} \\ M_{yy} \\ M_{xy} \end{Bmatrix} = \begin{bmatrix} D_{11} & D_{12} & 0 \\ D_{12} & D_{22} & 0 \\ 0 & 0 & D_{66} \end{bmatrix} \begin{Bmatrix} \varepsilon^1_{xx} \\ \varepsilon^1_{yy} \\ \gamma^1_{xy} \end{Bmatrix}$$
$$\begin{Bmatrix} Q_y \\ Q_x \end{Bmatrix} = K_s \begin{bmatrix} A_{44} & 0 \\ 0 & A_{55} \end{bmatrix} \begin{Bmatrix} \gamma^0_{xz} \\ \gamma^0_{yz} \end{Bmatrix}, \quad (A_{ij}, D_{ij}) = \int_{-h/2}^{h/2} Q_{ij}(1, z^2)\,\mathbf{d}z \tag{36}$$

where Q_{ij} are the plane stress-reduced elastic coefficients, which can be expressed in terms of the engineering constants E_1, E_2, G_{12}, G_{13}, G_{23}, and G_{13} as

$$Q_{11} = \frac{E_1}{1-\nu_{12}\nu_{21}},\ Q_{22} = \frac{E_1}{1-\nu_{12}\nu_{21}},\ Q_{12} = \frac{\nu_{21}E_1}{1-\nu_{12}\nu_{21}}$$
$$Q_{66} = G_{12},\ Q_{44} = G_{23},\ Q_{55} = G_{13} \tag{37}$$

3.2 Finite element model

The displacement finite element model of FSDT consists of five degrees of freedom per node $(u_0, v_0, w_0, \varphi_x, \varphi_y)$. The details of this development can be found in [3]. All variables are interpolated using equal interpolation, with the approximation functions being the tensor products of the one-dimensional spectral functions discussed in Section 2.3.

4 LINEARIZATION OF THE EQUATIONS

The linearization process can be accomplished with either of two techniques, namely the Picard (direct iteration procedure) or the Newton-Raphson's method. For checking the convergence behavior of both the methods of linearization with *hp*-spectral methods both of these were implemented. There was however, no difference found between the results of either of the methods for most cases and thus only results based on the Newton-Raphson's method will be presented. For all structural problems the Newton's method yields a symmetric positive definite matrix system which can be solved by conjugate gradient (Krylov subspace methods) solvers; the solver implemented for the solution of the above discrete problem is BPCG which can handle non-symmetric matrix systems with relative ease for the displacement based models. The mixed models were better handled with Gaussian elimination with scaled partial pivoting. Some of the advantages of the Newton-Raphson method are a faster convergence rate, since we are using incremental load steps for the runs, Newton's method does not noticeably outperform the Picard method of linearization in most cases. The Picard method faced some convergence issues for the pinned-pinned case for the mixed formulation and failed to converge even with an acceleration parameter. However the pinned-pinned problem with the displacement based FEM converged with the use of an appropriate acceleration parameter between the two successive iteration steps. The linearized problem with the Newton's method can be written as [3]

$$\mathbf{K}^{\mathrm{T}}(\boldsymbol{\Delta}^r)\,\delta\boldsymbol{\Delta} = -\mathbf{R}^r \equiv \mathbf{F} - \mathbf{K}(\boldsymbol{\Delta}^r)\boldsymbol{\Delta}^r \tag{38}$$

where $\mathbf{K}^{\mathrm{T}}$ denotes the tangent matrix, $\delta\mathbf{\Delta}$ is the increment of the solution, and $\mathbf{R}$ is the residual (or error) vector. The convergence criterion was set at a reduction in the L^2 norm of the residuals to a tolerance value of 10^{-06}, where as the convergence is declared when L^2 norm of the incremental vector normalized with the norm of the solution vector was less than 10^{-03} for the displacement based FEM models. The mixed FEM models were solved with Gaussian elimination with scaled partial pivoting, the non-linear residual convergence criterion was kept at the same values as reported for the displacement based *hp*-FEM model. In the forthcoming sections we present the results that we obtained for the linear and non-linear problems that were studied with different types of boundary conditions and also verify the spectral convergence of the solutions in the L^2 norm.

5 NUMERICAL RESULTS

5.1 Boundary conditions

Beams and plates with different boundary conditions are analyzed and results are obtained for linear and nonlinear bending. Various types of boundary conditions are summarized below.

$$\begin{aligned}&\text{Simply Supported Type SS1: } u_s = w_0 = \varphi_s = 0\\ &\text{Simply Supported Type SS3: } u_0 = v_0 = w_0 = 0\\ &\text{Clamped edge: } u_0 = v_0 = w_0 = \varphi_x = \varphi_y = 0\end{aligned} \tag{39}$$

The following load parameter is used to report the results:

$$\overline{P} = \frac{q_0 a^4}{E_2 h^4} \tag{40}$$

5.2 Discussion of results for beams

There are some advantages of the displacement based model over the mixed model that was discussed in Section 2.2. The displacement based finite element model [3] leads to a simpler system of equations from the matrix inversion point of view as the terms are all equal order. However, the mixed model, with stress resultants as the nodal variables, has disparate order terms which cause the model to experience convergence problems with the standard iterative solvers. Direct solvers were found to be able to parse the matrix system with relative ease. As for the solutions are concerned, the mixed model yields nodal values of the stress resultants whereas in the displacement model they are computed in the post-computation at the Gauss points. The mixed model tends to give better accuracy for the stress resultants. Fig. 1 shows the agreement between the *hp*/spectral results with the analytical solutions to the TBT beam. As is evident from the figure there is excellent agreement between both the slopes and deflections along the length of the beam with the analytical solutions. The non-dimensional deflections of the TBT beam subject to different loadings and increasing slenderness ratios have been presented in Fig. 2 for the pinned-pinned boundary condition, while Fig. 3 presents the non-dimensional deflections of the TBT beam subject to clamped-clamped boundary condition and increasing slenderness ratios.

5.3 Results for plates

In this section we present the results for a set of boundary conditions and for both isotropic and orthotropic plates. Both uniform and skewed meshes are used to determine their effect on the solutions. Exploiting the symmetry of the plate, only a quarter of the plate is modeled in most cases. The simply supported boundary condition of the SS1 type is used to obtain solutions to the problem and compared with analytical solutions. A uniform 2×2 *hp*-spectral discretization with $p = 8$ is used for side-to-thickness ratio, a/h, of 10, and a non-uniform 8×8 mesh with $p = 4$ is used for an a/h =100. The finite element solutions for deflections and stresses (not presented here) are found to be in excellent agreement with the analytical solutions [2]. No shear locking is apparent in the results obtained.

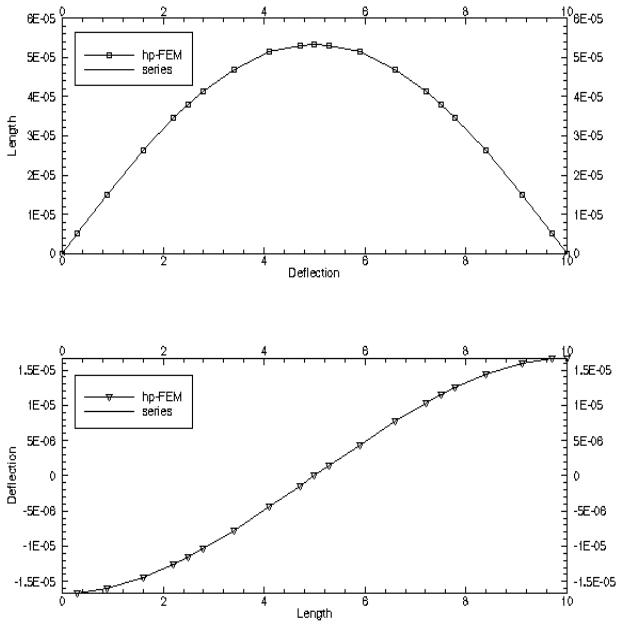

Fig 1
Agreement between the *hp*-FEM results and series solutions for the TBT.

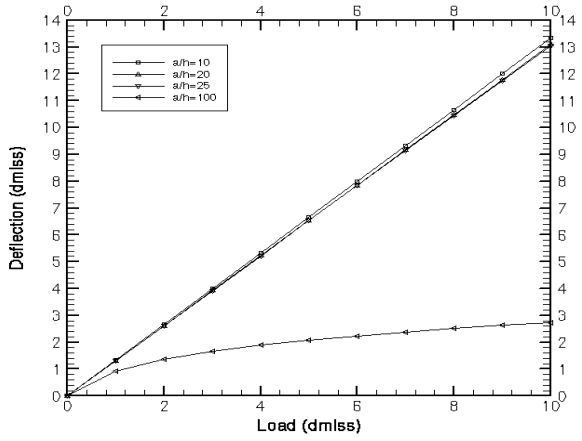

Fig 2
Load vs. non-dimensional deflection curves for Pinned-Pinned TBT beam for different slenderness ratios.

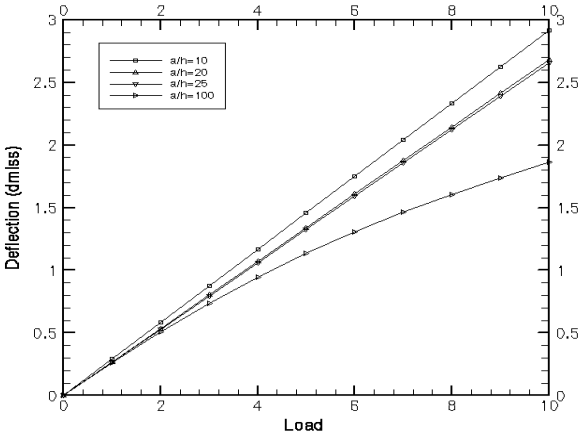

Fig 3
Load vs. non-dimensional deflection curves for CC TBT beam for different slenderness ratios.

It should be noted that the use of spectral functions with the Guass-Lobotto integration points allow the determination of stresses at the nodes because integration points coincide with the nodes of the plate. Thus, the displacements and stresses are computed at the geometric center of the plate. An orthotropic square plate subjected to uniformly distributed load of intensity q_0 is considered under SS1 and SS3 boundary conditions. The geometric and material parameter values that characterize the plate are;

$$a = b = 10 \text{ in.}, h = 0.138 \text{ in.}, E_1 = 3.0 \times 106 \text{ psi}, E_2 = 1.28 \times 106 \text{ psi}, G_{12} = G_{13} = G_{23} = 0.37 \times 106 \text{ psi}, \nu_{12} = 0.32 \tag{41}$$

An 8×8 spectral mesh with 1,089 nodes and 5,445 degrees of freedom was used in the analysis. Fig. 4 shows both 6×6 and 8×8 meshes. Convergence of the nonlinear solution was declared when the L^2 norm was less than 10^{-03} and the matrix solution convergence was declared when the L^2 norm of the residuals was less than 10^{-06}. For this analysis the Newton-Raphson iterative method [3] was used to solve the nonlinear equations. The problem typically required between 3 to 6 iterations for convergence. The results obtained with spectral approximations as well as those obtained with the conventional finite element (i.e., with low-order expansions and reduced integration) are included in Table 1. Next, the effect of skewed spectral mesh on the plate response is investigated. An orthotropic plate with material properties given in Eq. (41) and SS1 boundary conditions was analyzed with the 8×8 mesh shown in Fig. 4. Table 2 contains the results of the analysis. As can be seen from the results, distorted mesh does not have significant effect on the accuracy of the computed results. Fig. 5 contains plots of the center deflection as a function of the load parameter P for an isotropic plate. The SS3 and CC boundary conditions were used. Fig. 6 presents the stress vs. load parameter for the same problem. The 6×6 mesh shown in Fig. 4 is used to obtain the results.

Table 1
Orthotropic plate results

Results	SS3		SS1	
P	w_0	σ_{xx}	w_0	σ_{xx}
0.05	0.0030	0.4544	0.0030	0.4494
0.10	0.0060	0.9141	0.0060	0.9041
0.20	0.0119	1.8456	0.0120	1.8257
0.40	0.0236	3.7307	0.0237	3.6904
0.60	0.0348	5.5984	0.0348	5.5403
0.80	0.0453	7.4096	0.0454	7.3341
1.00	0.0552	9.1383	0.0552	9.0470
1.20	0.0643	10.7718	0.0643	10.6682
1.40	0.0727	12.3153	0.0727	12.1972
1.60	0.0805	13.7586	0.0806	13.6295
1.80	0.0881	15.1615	0.0879	14.9855
2.00	0.0949	16.4386	0.0947	16.2583
4.00	0.1466	26.3920	0.1455	26.0928
6.00	0.1795	33.1351	0.1796	32.9667
8.00	0.2054	38.6526	0.2054	38.3693
10.00	0.2267	43.3659	0.2265	42.9539
12.00	0.2462	47.7959	0.2448	47.1947
14.00	0.2618	51.5432	0.2608	51.1019
16.00	0.2760	55.1212	0.2752	54.7676
18.00	0.2891	58.5741	0.2884	58.1842
20.00	0.3011	61.8126	0.3005	61.4079
22.00	0.3123	64.9234	0.3117	64.4918
24.00	0.3227	67.8604	0.3223	67.4446

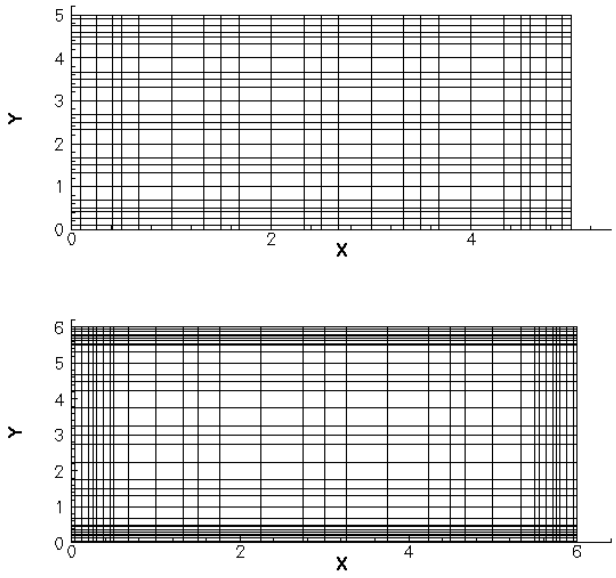

Fig 4
6×6 and 8×8 *hp*/spectral meshes used for solving non-linear isotropic and orthotropic plate problems.

Table 2
Skewed mesh results vs. straight mesh

	Skewed mesh		Regular mesh	
P	w_0	σ_{xx}	w_0	σ_{xx}
0.05	0.0112	1.0715	0.0112	1.0724
0.10	0.0224	2.1467	0.0224	2.1495
0.20	0.0438	4.2545	0.0438	4.2604
0.30	0.0636	6.2393	0.0636	6.2330
0.40	0.0815	8.0440	0.0815	8.0472
0.50	0.0976	9.6782	0.0976	9.6739
0.60	0.1122	11.1739	0.1122	11.1570
0.70	0.1255	12.4775	0.1255	12.4430
0.80	0.1382	13.7507	0.1382	13.6495
0.90	0.1492	14.7966	0.1492	14.8382
1.00	0.1596	15.8112	0.1596	15.8089
1.10	0.1693	16.7230	0.1693	16.7185
1.20	0.1785	17.6126	0.1785	17.6151
1.30	0.1871	18.4448	0.1871	18.3689
1.40	0.1952	19.1858	0.1952	19.0488
1.50	0.2030	19.9645	0.2030	19.9596
1.60	0.2104	20.7010	0.2104	20.7772
1.70	0.2175	21.3376	0.2175	21.2264
1.80	0.2243	22.0986	0.2242	21.8133
1.90	0.2308	22.7217	0.2308	22.7114
2.00	0.2371	23.4157	0.2371	23.0114

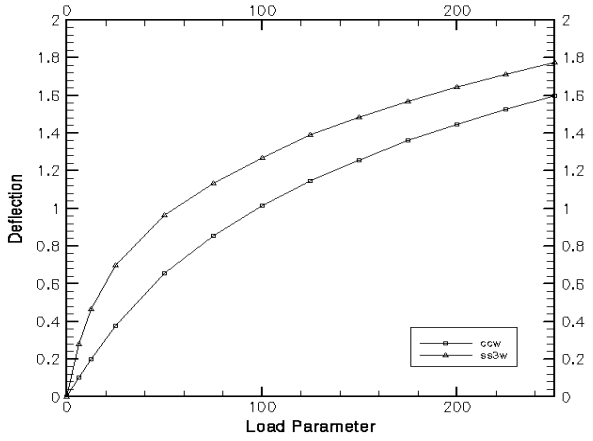

Fig 5
Load parameter vs. deflection curves for isotropic plate with CC and SS3 boundary conditions.

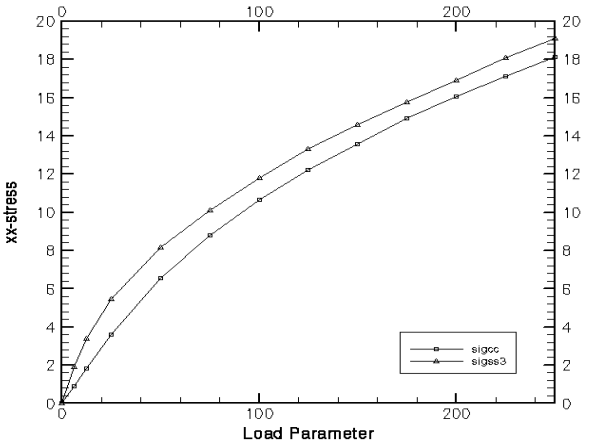

Fig 6
Load parameter vs. σ_{xx} for isotropic plate with CC and SS3 boundary conditions.

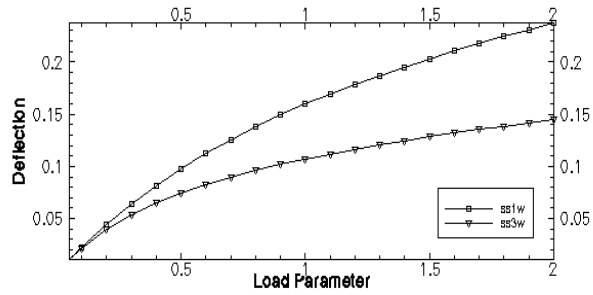

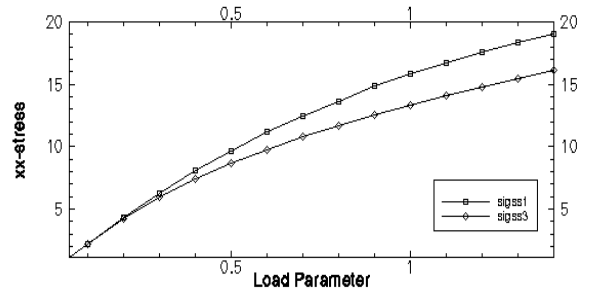

Fig 7
Load parameter vs. deflection and stresses for SS1 and SS3 boundary conditions for an orthotropic plate.

Fig. 7 presents nondimensionalized center deflection $\bar{w}_0 = w_0 / h$ and stress $\bar{\sigma}_{xx} = \sigma_{xx}(a^2 / Eh^2)$ as a function of the load parameter for orthotropic plates with SS1 and SS3 boundary conditions. The material properties used for this analysis are the same as those in Eq. (41). Fig. 8 presents the nondimensional deflections and stresses at the center of a clamped orthotropic plate as a function of the load parameter. Fig. 9 presents contains contour plots of the fields $(\varphi_x, \sigma_{xx}, \sigma_{yy})$ for an isotropic plate under uniform load and SS1 boundary conditions. Only quarter plate model is used. The plots correspond to the parameter of 250. The stresses σ_{xx} and σ_{yy} were calculated at the top of the plate ($z = h/2$), where as the stress σ_{xy} was calculated at the bottom of the plate ($z = -h/2$). Fig. 10 presents the same variables as Fig. 9 but for an orthotropic plate under uniform load (load parameter $P = 2.0$) and SS1 boundary conditions. As can be seen from Figs. 9 and 10, these fields develop differently for isotropic and orthotropic plates.

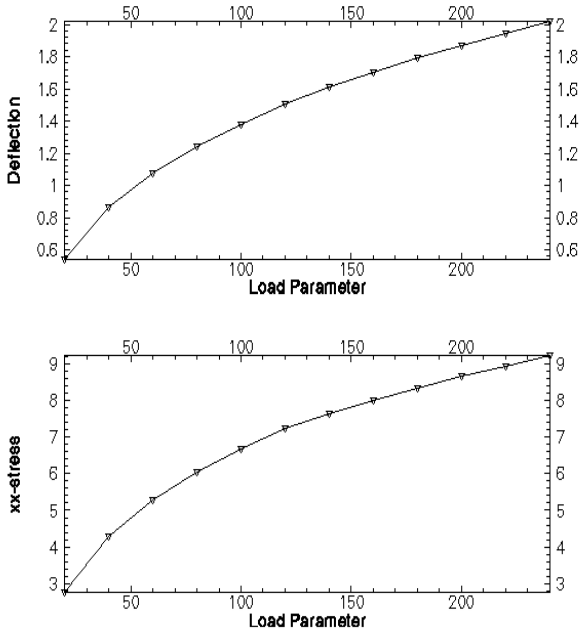

Fig 8
Load parameter vs. deflection and stresses for clamped (on all edges) orthotropic plate.

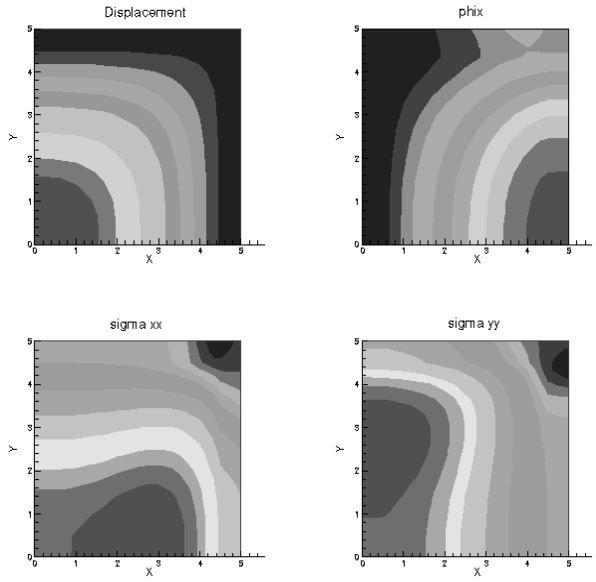

Fig 9
Contour plots of $(\varphi_x, \sigma_{xx}, \sigma_{yy})$ fields for an isotropic plate subject to SS1 boundary conditions.

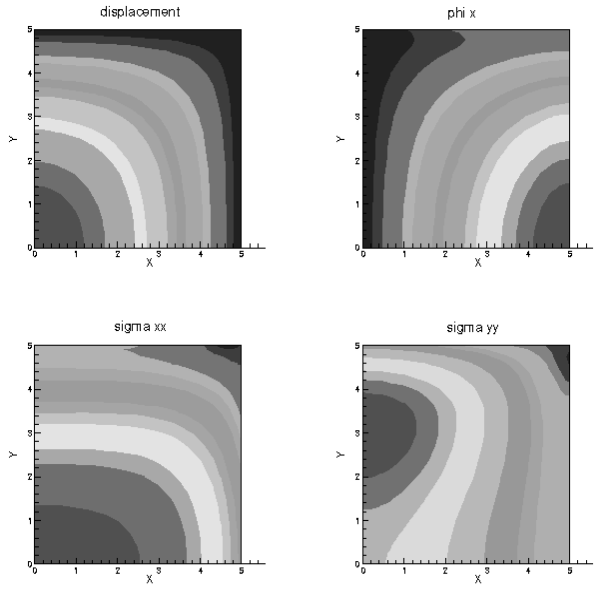

Fig 10
Contour plots of $(\varphi_x, \sigma_{xx}, \sigma_{yy})$ fields for an orthotropic plate subject to SS1 boundary conditions.

6 CONCLUSIONS

Through this work we have demonstrated the usage of spectral finite element approximations as a viable tool for predicting the bending response of shear deformable beams and plates using the Timoshenko beam theory and the first-order shear deformation plate theory. Both linear and non-linear problems were solved on straight and skewed meshes. We also advocate the usage of higher order spectral basis with full integration for predicting the bending response without the use of ad-hoc procedures of reduced and selective integration to obtain reliable results for both linear and non-linear problems. Possible extensions of this work are in using *hp*-spectral methods for modeling composite laminated plates and shells.

REFERENCES

[1] Reddy J.N., 2004, *Mechanics of Laminated Composite Plates and Shells*, CRC Press, Boca Raton, FL, Second Edition.
[2] Reddy J.N., 2007, *Theory and Analysis of Elastic Plates and Shells*, CRC Press, Boca Raton, FL, Second Edition.
[3] Reddy J.N., 2004, *An Introduction to Non-Linear Finite Element Analysis*, Oxford University Press, Oxford, UK.
[4] Donning B.M., Liu W.K., 1998, Meshless methods for shear-deformable beams and plates, *Computer Methods in Applied Mechanical Engineering* **152**: 47-71.
[5] Maenghyo C., Parmerter R., 1994, Finite Element for composite bending based on efficient higher order theory, *AIAA Journal* **32**: 2241-2248.
[6] Pontaza J.P., Reddy J.N., 2004, Mixed plate bending elements based on least squares formulations, *International Journal for Numerical Methods in Engineering* **60**: 891-922.
[7] Urathaler Y., Reddy J.N., 2008, A mixed finite element for nonlinear bending analysis of laminated composite plates based on FSDT, *Mechanics of Advanced Materials and Structures* **15**: 335-354.
[8] Archiniega R.A., Reddy J.N., 2007, Large deformation analysis of functionally graded shells, *International Journal for Solids and Structures* **44**: 2036-2052.
[9] Karniadakis G.K., Sherwin S., 2004, Spectral/*hp* element methods for computational fluid dynamics, Oxford Science Publications, London, Second Edition.
[10] Melenk J.M., 2002, On condition numbers in *hp*-fem with Gauss-Lobatto-based shape functions, *Journal of Computational and Applied Mathematics* **139**: 21-48.
[11] Maitre J.F., Pourquier O., 1996, Condition number and diagonal preconditioning: comparison of the *p*-version and the spectral element methods, *Numerical Methods* **74**: 69-84.
[12] Reddy J.N., 1997, On Locking-free shear deformable beam finite elements, *Computer Methods in Applied Mechanics and Engineering* **149**: 113-132.

[13] Reddy J.N., Wang, C.M., Lam, K.Y., 1997, Unified finite elements based on the classical and shear deformation theories of beams and axisymmetric circular plates, Communications in Numerical Methods in Engineering **13**: 495-510.
[14] Reddy J.N., 2006, *An Introduction to the Finite Element Method*, McGraw-Hill, New York, Third Edition.
[15] Prabhakar V., Reddy, J.N., 2007, Orthogonality of modal basis in *hp* finite element models, *International Journal for Numerical Methods in Fluids* **54**: 1291-1312.
[16] Osilenker B., 1999, *Fourier Series in Orthogonal Polynomials*, World Scientific, Singapore, Second Edition.
[17] Reddy, J.N., 2002, *Energy Principles and Variational Methods in Applied Mechanics*, John Wiley & Sons, New York.